Supporting Information

Near-Edge Ligand Stripping and Robust Radiative Exciton Recombination in CdSe/CdS Core/Crown Nanoplatelets

Jari Leemans,[†,‡] Shalini Singh,[†,‡] Chen Li,[¶] Stephanie Ten Brinck,[§] Sara Bals,[¶] Ivan Infante,[‖,⊥] Iwan Moreels,[†,‡] and Zeger Hens[*,†,‡]

†*Physics and Chemistry of Nanostructures, Ghent University, 9000-Ghent, Belgium*

‡*Center for Nano and Biophotonics, Ghent University, 9000-Ghent, Belgium*

¶*Electron Microscopy for Materials Research (EMAT), University of Antwerp, Groenenborgerlaan 171, 2020 Antwerp, Belgium*

§*Department of Theoretical Chemistry, Faculty of Science, Vrije Universiteit Amsterdam, de Boelelaan 1083, 1081 HV Amsterdam, The Netherlands*

‖*Department of Nanochemistry, Istituto Italiano di Tecnologia, Via Morego 30, 16163 Genova, Italy*

⊥*Department of Theoretical Chemistry and Amsterdam Center for Multiscale Modeling (ACMM), VU University Amsterdam, 1081 HV Amsterdam, The Netherlands*

E-mail: zeger.hens@ugent.be

S1 Experimental Section

S1.1 Chemicals

Cadmium nitrate tetrahydrate ($Cd(NO_3)_2.4H_2O$, 98%), sodium myristate (Na(myr)), CdO (99.99%), sulphur (flakes), Cadmium acetate dihydrate ($Cd(OAc)_2.2H_2O$, 98%), octanoic acid, butylamine ($BuNH_2$) and N,N,N',N'-tetramethylethylenediamine (TMEDA) were purchased from Sigma Aldrich. Selenium powder (200-mesh) was purchased from Acros organics. Oleic acid (90% tech.) and 1-octadecene (ODE, 90%) were purchased from Alfa Aesar. Methanol (MeOH), ethanol (EtOH), and hexane were purchased from Fiers.

S1.2 Preparation of Cadmium Myristate ($Cd(myr)_2$)

$Cd(NO_3)_2.4H_2O$ (3 g, 9.72 mmol) is dissolved in 200 mL MeOH. Na(myr) (5 g, 20 mmol) is dissolved in 500 mL MeOH. Dropwise and whilst stirring, the cadmium nitrate solution is added to the Na(myr) solution. After 2 hours of stirring, the white precipitate is filtered off with a buechner filter and filter paper. The wet collected precipitate ($Cd(myr)_2$) is washed 3 times with MeOH. The wet $Cd(myr)_2$ is dried under vacuum for 24 hours and stored in the fridge until use.

S1.3 Preparation of Cadmium Oleate ($Cd(Ol)_2$)/ODE Mixture

CdO (1.926 g, 15 mmol) is combined with oleic acid (15 mL, 45 mmol) in 1-octadecene (ODE, 15 mL). The mixture is degassed under vacuum at 80°C for 1 hour. Afterwards, the solution is heated to 150°C under inert atmosphere. Upon achieving complete transparancy (approximately 15minutes), CdO has been fully transformed to cadmium oleate ($Cd(ol)_2$) and the mixture is cooled and poured into vials for storage until use. The mixture solidifies at room temperature so the wax is melted prior to use.

S1.4 Synthesis of 4.5 ML CdSe NPLs

$Cd(myr)_2$ (340 mg, 0.6 mmol), Se (24 mg, 0.3 mmol) and ODE (25 mL) are combined in a 3-neck flask equipped with stirring bar, temperature sensor, heating mantle and a condenser that is connected to a schlenk line. The solution is degassed under vacuum for 30 minutes at 90°C. After degassing, it is heated to 240°C under inert atmosphere. During the temperature ramp around 215°C, when the solution has turned orange, $Cd(OAc)_2.2H_2O$ (80mg, 0.3mmol) is added by swiftly opening the reaction vessel, adding the powder and closing the septum again. The reaction is left to proceed for 6 minutes at 240°C, after which 1g of the Cd-oleate/ODE mixture is injected to quench the reaction. The heating mantle is removed and the mixture cooled to room temperature. The NPLs are washed by a single precipitation with hexane/EtOH and redispersed in hexane for storage. The NPLs are small with average lateral dimensions of 17×6 nm.

S1.5 Preparation of the CdS Crown Growth Solution

Dissolve elemental S (0.0481 g, 1.5 mmol) in 9 mL ODE. In a separate vial, combine 6 mL ODE with CdO (0.27 g, 2.1 mmol) and 950 μL octanoic acid (6 mmol). Under nitrogen and whilst stirring, heat to 150°C until the reddish brown color of CdO disappears and cadmium octanoate ($Cd(oct)_2$) has been formed. Cool the solution to 90°C to keep the $Cd(oct)_2$ dissolved and add the S solution. The CdS crown growth solution is a homogeneous solution above 90°C and is injected as such.

S1.6 Synthesis of Optimised CdS Crowns

With the use of the linear absorption coefficient determined in a separate report for our CdSe NPLs[1] according to Achtstein et al.,[2] the molar yield of the core synthesis is evaluated and the reagents and solvent are scaled accordingly for crown growth. The amounts presented here are optimised for 10 nmol of CdSe NPLs (ca. 1 synthesis) of average dimensions of

17×6 nm. 10 nmol CdSe NPLs are combined with 30 mL ODE, oleic acid (50 μL, 0.16 mmol) and $Cd(OAc)_2.2H_2O$ (0.266 g, 1 mmol) in a 3-neck flask. The mixture is degassed at 40°C for 1 hour, after which the flask is placed under inert atmosphere and heated to 200°C. At 200°C, 10mL of the slightly heated CdS crown growth solution is added for 40 minutes (15 mL/hr). A swift injection rate is essential for the homogeneous growth of CdS crowns. After 40 minutes of injection, the reaction is left to react for an additional 20 minutes until growth of CdS has stopped. The reaction is quenched by injection of 2 g of the melted $Cd(ol)_2$/ODE mixture, upon which the turbid mixture turns into a transparent colloidal dispersion that is luminescing green already under ambient lighting. After cooling below the boiling point of hexane, 10 mL of hexane is added to the flask to prevent stacking of the NPLs. The core/crown NPLs are purified via precipitation with EtOH and redispersion in hexane. The supernatant should be clear indicating that the entire ensemble has been precipitated. As such the consequent studies are representative of the entire reaction product and inherently serve as an evaluation of the synthetic protocol, not the purification procedure.

S1.7 Characterization/Electron Microscopy

The CdSe-CdS nano-plates (NPLs) were dropcasted on Cu TEM grids with ultra-thin carbon film. A FEI Osiris electron microscope was operated at 200 kV in the mode of scanning transmission electron microscopy (STEM) for taking high-angle annular dark-field (HAADF) images. A super-X Energy Dispersive X-ray (EDX) Detector installed at FEI Osiris was used to take EDX mappings on 19 NPLs, from which the Se and S line profiles were extracted. Bruker-Esprit software was used for EDX elemental analysis.

S1.8 Preparation of Titration Samples

Samples for nuclear magnetic resonance experiments and photoluminescence titration are prepared via 3 cycles of precipitation and redispersion. This ensures the absence of any unbound organic molecules or synthesis byproducts and allows the analysis of pure disper-

sions of core/crown NPLs and their surface bound ligands. After the 3rd redispersion the NMR samples are additionally dried under N_2 flow and dissolved in cyclohexane-d_{12}. Ligand stripping during a titration may cause NPL aggregation and precipitation, yet we found that NPL dispersions remain optically translucent within the first few hours after butyl amine addition. All data presented in the manuscript were recorded on such dispersions.

S1.9 NMR Titration

NMR measurements were recorded on a Bruker Avance III spectrometer operating at a 1H frequency of 500.13 MHz and equipped with a BBI-Z probe. Quantitative ^{1}H spectra were recorded with a 20 s delay between scans to allow full relaxation of the magnetisation. The initial concentration of surface bound ligands is determined according to the digital ERETIC method.[3] Consequently equivalents of $BuNH_2$ are calculated for the stripping experiment. The desorption is studied via repeated addition of the amine equivalent and consequent registering of the ERETIC spectrum under identical measurement conditions as the initial spectrum. The NMR spectra are processed in IGOR Pro, version 6.32.

S1.10 Density Functional Theory Simulations

Models were constructed by cutting a nonstoichiometric 5 ML nanoplatelet from the bulk, resulting in a 3.07 x 3.07 x 1.25 nm^3 NC. Resulting NPLs expose six (100) facets, with Cd-rich and Se/S-rich (111) facets at the vertices. Charge neutrality is maintained by added 194 chloride atoms to the surface, leading to a total atom count of 392 Cd atoms, 295 Se/S atoms and 194 Cl atoms. Density Functional Theory calculations were performed using the PBE exchange-correlation functional[4] and a double-ζ basis-set augmented with polarization functions[5] using the CP2k software package.[6] All structures were optimized in the gas phase.

S1.11 PL Titration

A thoroughly washed core/crown sample equal in concentration to the NMR titration sample is dispersed in 2mL of hexane. 10 μL of the stock solution is diluted to 3 mL and placed in a PL cuvette. The photoluminescence quantum yield (PLQY) is determined with an edinburgh FLS920 spectrometer equipped with an integrating sphere for absolute Quantum Yield determination. Afterwards the integrating sphere is removed and a standard luminescence setup is used. The slit widths, excitation wavelength and integration times are all fixed throughout the entire experiment so that PL intensities can be registered and when corrected for absorption can be used to calculate relative photoluminescence efficiencies. After the recording of the initial core/crown solution, the first equivalent of amine is added to the stock solution. When the mixture has been thoroughly shaken, 10 μL are removed, diluted to 3 mL with hexane and the photoluminescence spectrum is recorded. The sample is then transferred to an absorption cuvette and the absorption spectrum is recorded. Consequently, the next equivalent of amine is added to the stock solution, diluted, measured in PL and absorption until all titration steps have been registered.

The photoluminescence spectra are corrected by dividing by the integrated absorbance between 455 and 465 nm across the excitation wavelength of 460 nm that was used to excite the core during the PL titration. The absorbance corrected PL intensities are representative of relative PL efficiencies, and together with the absolute quantum yield of the initial sample can be used to calculate relative PLQY according to equation S1.

$$QY_x = QY_{ref} * \left(\frac{I_{PL,x}}{I_{A,x}}\right) * \left(\frac{I_{A,ref}}{I_{PL,ref}}\right) \tag{S1}$$

With I referring to the integrated PL and Absorbance intensities according to the subscript used.

S2 Analysis of CdS Crown Growth

S2.1 Absence of CdS Exciton Emission

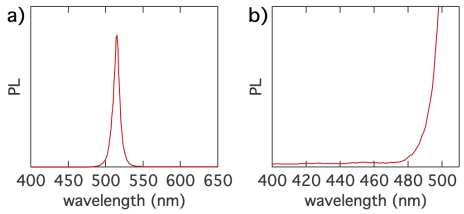

Figure S1: Photoluminescence spectrum for the core/crown CdSe/CdS NPLs when photoexciting at 370nm indicates no CdS emission.

In order to create excitons exclusively in the CdSe core, most photoluminescence studies in the main manuscript use photoexciting at 460 nm. However, to prove the absence of CdS NPL formation in the synthesis, shorter excitation wavelengths are needed to excite possible CdS excitons as well. Such a PL spectrum is presented in Figure S1a, while Figure S1b shows a magnfication of the baseline in the spectral range where CdS emission would be expected. No traces of CdS exciton emission are observed.

S2.2 Morphology of Optimized Core/Crown NPLs

To investigate the homogeneity of the core/crown morphology across an ensemble of NPLs, we imaged different NPLs using high angle annular dark field scanning STEM (HAADF-STEM), while simultaneously analyzing the local composition by energy dispersive x-ray spectroscopy (EDX). Due to the presence of residual ligands around the NPLs and the sensitivity of the NPLs to the electron beam, we restricted this STEM-EDX mapping to line profiles of Se and S along the long axis of a given NPL. In this way, a reasonable signal-to-noise ratio could be obtained despite the carbon contamination, whilst also avoiding sample damage. Out of a set of 19 NPLs, we found that 17 NPLs exhibited a CdS crown on both sides of the CdSe core, suggesting a complete lateral encapsulation of the core by the crown. A representative example of this NPL subset is shown in Figure S2a. Here, the line profile

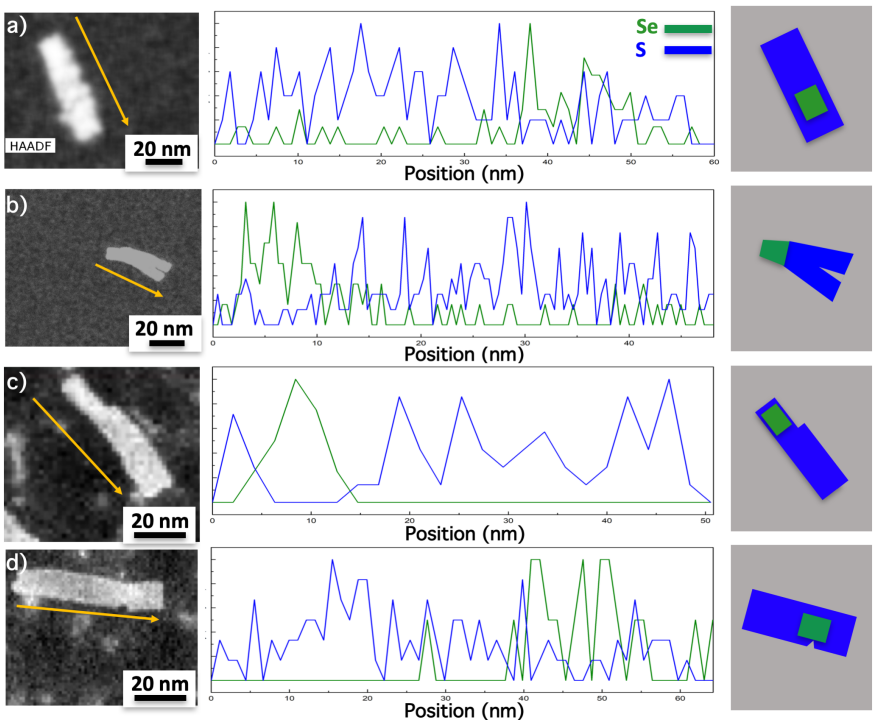

Figure S2

of S extends along the full NPL length, whereas the Se signal is restricted to a region that covers only part of the NPL. In line with the HAADF-STEM image of this NPL, such a line scan suggests a morphology as shown in Figure S2a, where an off-center CdSe core is embedded within a rectangular CdS crown. Figure S2b provides an example of a NPL not following this dominant picture. In this case, S is only detected at one side of the core Se, which indicates the formation of a partial crown. Furthermore, the STEM image even shows a split top surface on the other end of this NPL. Next to the completeness of the CdS crown, the HAADF-STEM images also enabled us to evaluate smaller deviations from the ideal core/crown morphology. Figure S2c, for example, shows a NPL for which the combination of the STEM-EDX map and the HAADF-STEM image suggests a morphology in which a narrow, CdSe-rich side is combined by a wider, one-sided CdS crown. The NPL depicted in Figure S2d, on the other hand, features an indent at the height of the CdSe core, possibly exposing the CdSe edge to the surroundings. Additional examples of NPLs featuring crowns with such minor defects, such as bends and indents, are given in Figure S3.

Based on this TEM analysis, we conclude that the core/crown synthesis leads on average to the formation of a sizeable CdS crown on each CdSe edge. However, notwithstanding this average core/crown morphology, it appears that an entire ensemble still contains a significant fraction of defective core/crown NPLs with partially exposed CdSe edges. These observed defects fall in line with the conclusions drawn from the photophysical properties of the ensemble in the main manuscript.

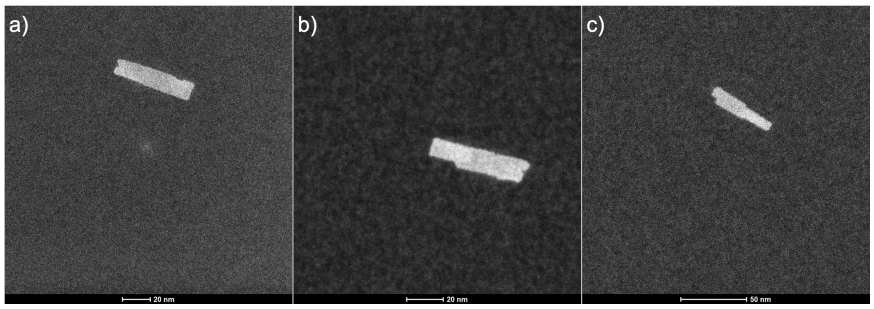

Figure S3: Additional HAADF-STEM images of CdSe/CdS core/crown NPLs synthesized using the optimized procedure, featuring CdS crowns with (a) a local indent, (b) a single shift of the crown thickness and (c) multiple variations of the CdS crown thickness.

S2.3 Synthesis and Analysis of Defective Core/Crown NPLs

The non-optimized core/crown NPLs that do not display robust photoluminescence at high ligand stripping are synthesized with the same procedure as the optimized NPLs, except for the amount of Cd/S growth solution, which was reduced to 3 mL per 10 nmol of CdSe cores. The absorption spectrum shown in Figure S4a displays the expected CdSe and CdS exciton absorption features. TEM imaging, on the other hand, indicates that these NPLs have less rectangular shapes than the optimized samples, see Figure S4b. Even so, a sizing analysis based on bright-field TEM images indicates that the length of the NPLs grows by 8 nm, whereas the thickness increases by 1 nm on average, see histograms in Figures S4c-d. More precisely, the average NPL grows from measuring $20 \times 6 \times 1.2$ nm to $28 \times 7 \times 1.2$ nm. From the PL titration data shown in Figure 3a, it follows that such crown dimensions are insufficient to achieve robust photoluminescence.

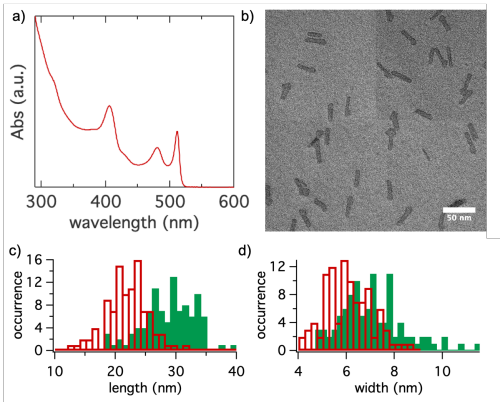

Figure S4: a) Absorption and b) TEM image of the non-optimized core/crown NPLs referenced in the NMR data and PL tests in the main manuscript. c) and d) Histograms of the sizes of the cores (red) and non-optimized core/crown sample (green) obtained from TEM micrographs. A clear increase in the length and a limited widening of the NPLs during CdS crown growth is visible.

S3 Data and Models for $BuNH_2$ Induced $Cd(Ol)_2$ Stripping

S3.1 Determination of Desorbed $Cd(Ol)_2$ Fraction

1D ^{1}H NMR spectra are phased and background corrected prior to quantification. After recording, the intensity of all spectra during the titration is corrected for dilution and receiver gain of the NMR magnet. The experimental isotherm is then obtained from the NMR spectra by integrating the emerging α-CH_2 resonance as a measure for the desorbed oleate fraction as indicated in Figure S5. This is accomplished by fitting the resonance feature on top of a background. The desorbed fraction is obtained by dividing this integrated area by the area of the methyl resonance of the pure sample, which provides a commensurate measure of the total ligand concentration. The bound fraction corresponds to 1 minus this value. The fits are illustrated in Figure S5 and the data are summarized in Table S1.

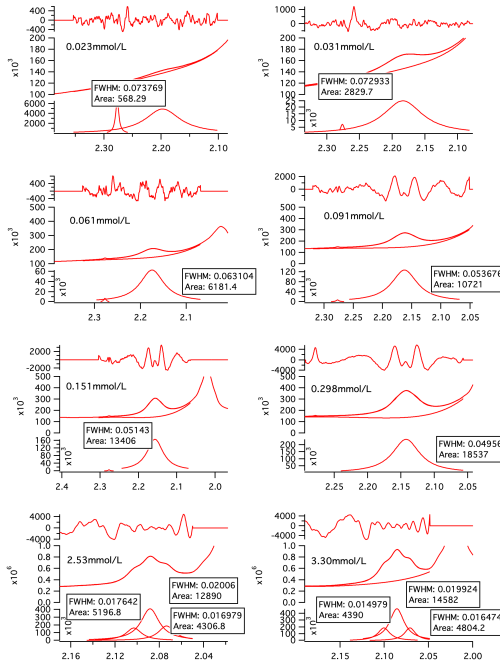

Figure S5: Representation of how the intensity of the α-CH_2 resonance is extracted from the background of the neighboring feature.

S3.2 Coupled Equilibrium Treatment for the Two-Site Model

The two-site model involves a coupled equilibrium between two different surface binding sites. This allows for the derivation of an expression of equilibrium concentrations for all partaking reactants and products, which are needed in the equilibrium constant expressions. To solve the system of coupled chemical equilibria S2 and S3, the degree of advancement γ and δ for the respective reactions are introduced. In Table S2, this approach is illustrated which yields expressions for the equilibrium concentrations of the reactants and products at the bottom of the table.

$$[\mathrm{CdX}](\mathrm{Cd(Ol)_2})_1 + 2\mathrm{BuNH_2} \rightleftharpoons [\mathrm{CdX}](\circ)_1 + \mathrm{Cd(Ol)_2} - (\mathrm{BuNH_2})_2 \tag{S2}$$

$$[\mathrm{CdX}](\mathrm{Cd(Ol)_2})_2 + 2\mathrm{BuNH_2} \rightleftharpoons [\mathrm{CdX}](\circ)_2 + \mathrm{Cd(Ol)_2} - (\mathrm{BuNH_2})_2 \tag{S3}$$

The equations for the equilibrium constants K_1 and K_2 with the expressions for the

Table S1: Data from the fitting of the alpha-CH_2 resonance and the calculated bound fractions

α-CH_2 area/2	total CH_3 area/3	bound fraction	mmol.L^{-1} $BuNH_2$	equivalents amine
0	23580 ± 77.74	1	0	0
284.1 ± 24.729		0.988	0.023	1.5
1415 ± 28.213		0.940	0.031	2
3091 ± 19.379		0.869	0.061	4
5361 ± 37.349		0.773	0.091	6
6703 ± 65.925		0.716	0.151	10
9269 ± 112.04		0.607	0.298	20
11196 ± 125.31		0.525	2.53	220
11888 ± 121.23		0.496	3.30	320

Table S2: Table layout indicating how the coupled equilibrium is solved to obtain equilibrium concentrations necessary for the equilibrium expressions.

advancement	$[CdX]Z_1$	$[CdX]Z_2$	$BuNH_2$	$[CdX](\circ)_1$	$[CdX](\circ)_2$	$Z-(BuNH_2)_2$
0	$Z_{1,0}$	$Z_{2,0}$	L_0	0	0	0
γ	-γ		-2γ	+γ		+γ
δ		-δ	-2δ		+δ	+δ
equilibrium	$Z_{1,0}$-γ	$Z_{2,0}$-δ	L_0-2γ-2δ	γ	δ	γ+δ

equilibrium concentrations in terms of γ and δ become:

$$K_1 = \frac{\gamma(\gamma+\delta)}{(Z_{1,0}-\gamma)(L_0-2(\gamma+\delta))^2} \tag{S4}$$

$$K_2 = \frac{\delta(\gamma+\delta)}{(Z_{2,0}-\gamma)(L_0-2(\gamma+\delta))^2} \tag{S5}$$

To extract a theoretical binding profile to match the experimental data, the set of coupled equations S4 and S5 must be solved for γ and δ at different added amine concentration L_0. To do so, an estimate of α, K_1 and K_2 are chosen. Here, α is the fraction of all binding sites classified as site 1:

$$Z_{1,0} = \alpha * Z_{tot} \tag{S6}$$

$$Z_{tot} = Z_{1,0} + Z_{2,0} \tag{S7}$$

Now all parameters in the equations are either known or estimated except for γ and δ. These can be solved for with the 2 equilibrium constant equations at each amine concentration from the titration experiment. The desorbed fraction that is plotted on top of the experimental data is obtained by dividing the sum of γ and δ by the total ligand concentration Z_{tot} obtained from an ERETIC 1H-NMR measurement. The 3 chosen parameters α, K_1 and K_2 are set such that the simulated desorption profile matches the experimental profile. The final values of α, K_1 and K_2 are then taken as descriptors of the binding site heterogeneity on the nanoplatelet surface as discussed in the main text.

S3.3 A Geometric Benchmark for the Fraction of (Near)-Edge Sites

To obtain a benchmark value for α, *i.e.*, the fraction of weakly binding surface sites on the core/crown NPLs, we rely on the DFT results which suggests that binding sites can be roughly split in two groups. A first, the edge and nearest-neighbor edge sites, are characterized by a broad distribution of binding energies that is, overall, significantly smaller than the binding sites on the center of a facet. Taking a lattice parameter of 0.6 nm – a number in between the lattice parameter of CdSe and CdS, we can calculate the corresponding fraction of weak binding sites assuming a core/crown NPL with a rectangular shape. Using the average dimensions of the NPLs used for the NMR titration ($28.6 \times 7 \times 1.2\,\mathrm{nm}$, we thus obtain a total NPL area of $490\,\mathrm{nm}^2$ and an inner (facet) area of $323\,\mathrm{nm}^2$. This figures yield a fraction of weak binding sites $\alpha = 0.34$. Since shifts of the crown thickness or indents in the crown will increase the relative number of (near)-edge sites, this number probably underestimates

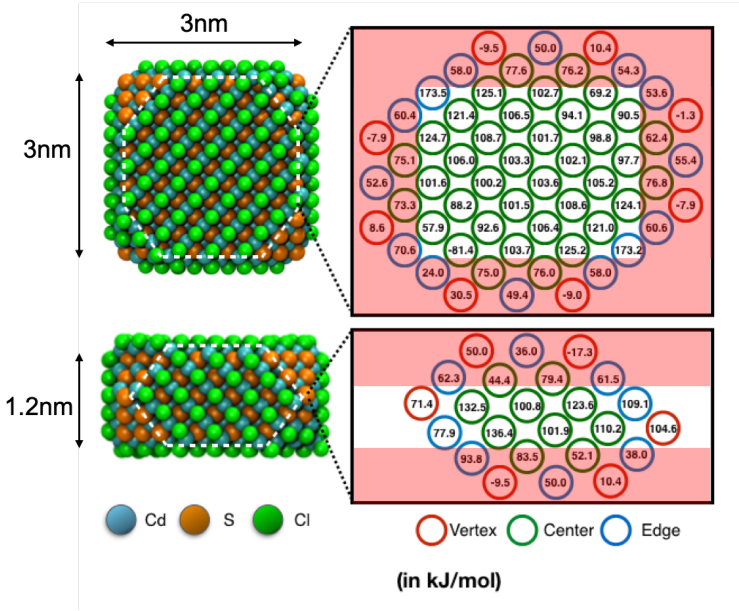

Figure S6: The binding sites on the DFT model can be roughly distributed into edge sites and bulk sites based on the desorption energy for the corresponding amine induced displacement. After approximately two atomic lines that desorption energy reaches a constant value as would be expected for coordination on a flat surface.

the actual fraction of weak binding sites.

S3.4 Computed Displacement Energies

The computational reaction energies for the displacement of $CdCl_2$ from relevant model NPLs are represented as histograms in Figure 2 of the main text. The individual desorption energies are here superposed on the corresponding surface sites in Figure S7. The site-independent desorption energies in the center of the facets forms a basis of our argumentation.

S3.5 X-ray Fluorescence Analysis during $BuNH_2$ Titration

X-ray fluorescence spectroscopy (XRF) was used to corroborate the loss of $Cd(Ol)_2$ upon $BuNH_2$ addition according to Eq 1 from the main manuscript. According to that equation, $BuNH_2$ addition should reduce the Cd:Se ratio in the NPLs, whilst only Cd should be detectable in the supernatant when precipitating a butylamine treated sample. For this

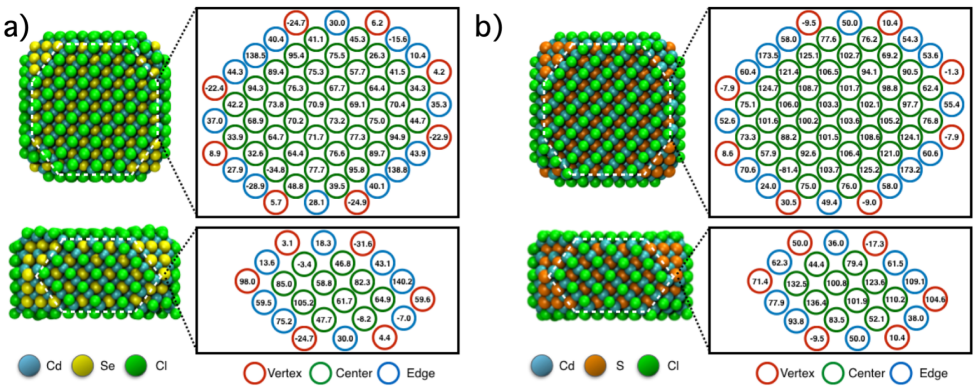

Figure S7: Desorption energies for the displacement of $CdCl_2$ according to equation 4 in the main text superposed on the corresponding a) CdSe and b) CdS NPL.

analysis, we first cast part of a core/crown NPL sample on an XRF-compatible substrate and analyzed its elemental composition. Next, an excess of butylamine was added to the remaining dispersion after which NPLs aggregation was induced by addition of ethanol as the non-solvent. The aggregated NPLs and the supernatant were separated by centrifugation, and the dry NPL pellet was redispersed in hexane. Again, that sample was cast on a substrate and its composition analysed by XRF. Finally, the supernatant was dried slowly on top of a substrate and the resulting residue was also analysed with XRF. The results are presented in Figure S8. One sees that the ratio of the integrated Cd/Se K_α signals reduces by 3% when treating the sample with butylamine, a result indicating a preferential loss of Cd. Moreover, the XRF spectrum of the supernatant only features Cd-K_α fluorescence, without any trace of

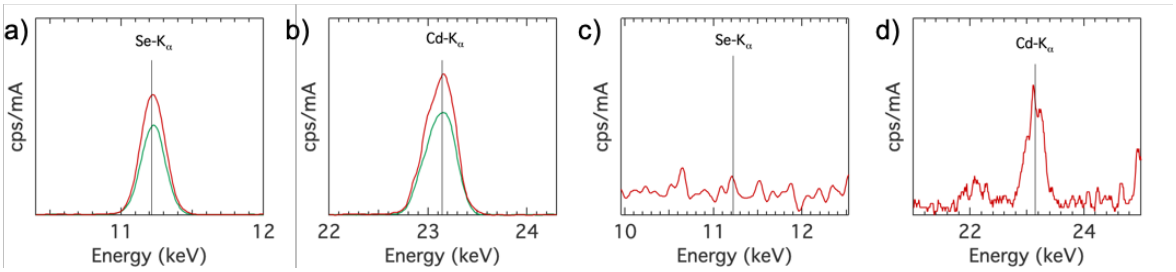

Figure S8: XRF spectra for the CdSe/CdS NPLs (green) before and (red) after ligand stripping and purification around the a) Se-K_α and b) Cd-K_α peak. The supernatant of the purification was also analysed and along with the displacement of cadmium oleate during stripping, c) no Se was found but d) Cd was clearly present.

selenium. This analysis confirms that Cd desorbs alongside the oleate identified with NMR.

S4 Steady-state and Transient Photoluminescence Spectroscopy

S4.1 Preferred Quenching of the Blue Side of the Emission Line

Overlaying the PL spectra before and after $BuNH_2$ titration reveals a preferential quenching of the blue side of the PL signal. This falls in line with the quenching of the incompletely crowned fraction of the ensemble as the will, on average, have experienced less of a red-shift during crown growth.

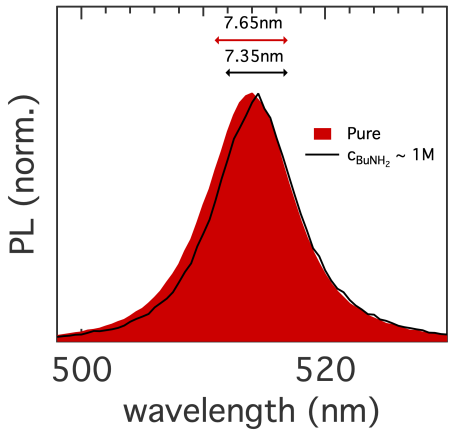

Figure S9: Overlaid photoluminescence spectra before and after addition of 1M of $BuNH_2$.

S4.2 Analysis of the Photoluminescence Decay Traces

We analyzed the photoluminescence decay traces by fitting the logarithm of the counts to the logarithm of the sum of 3 exponentials (see Eq S8). The background level A_0 was estimated from the measured intensity before excitation and kept fixed during the fitting. To avoid erroneous fits for the initial part of the trace, the amplitude of the first component was fixed at 1. Given the small values of A_2 and A_3, this approach only induced minor errors.

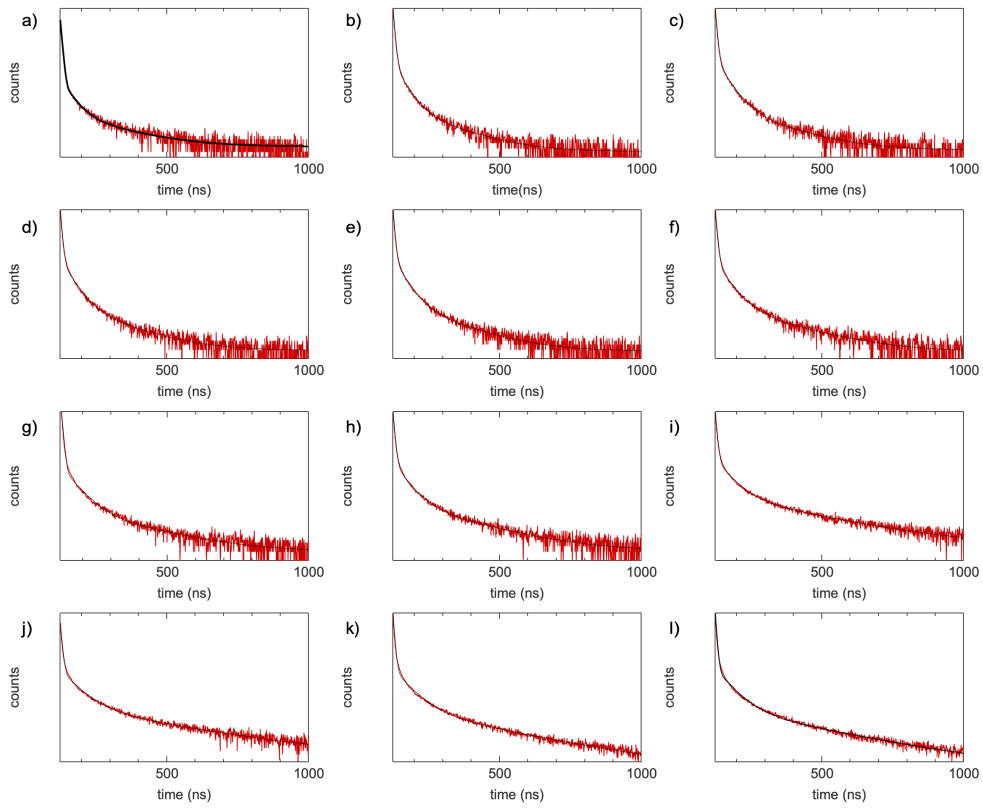

Figure S10: a)-l) The transient photoluminescence data points (red) with the fitted 3 exponential decay (black line) in order of increasing concentration of $BuNH_2$.

The parameters from the fits were used to estimate the integrated intensity, after which all traces and amplitudes were rescaled such that the integrated intensity was proportional to the quantum yield of the sample. The fitted traces and extracted constants are displayed in Figure S10 and Table S3, respectively.

$$I(t) = A_0 + A_1 e^{-k_1 t} + A_2 e^{-k_2 t} + A_3 e^{-k_3 t} \tag{S8}$$

Using the rates and the amplitudes, we estimate the contribution f_i of each component i to the total emission intensity as:

$$f_i = \frac{A_i k_i^{-1}}{\sum_i A_i k_i^{-1}} \tag{S9}$$

The resulting fractions have been summarized in Table S4. It follows that 95% of the

Table S3: Parameters obtained from the fit of each TRPL trace.

[$BuNH_2$] (mM)	k_1 (ns^{-1})	k_2 (ns^{-1})	k_3 (ns^{-1})	A_1	A_2	A_3	A_0
0	0.274	0.0354	0.0073	1	0.0049	0.00029	$1.57\ 10^{-5}$
2.53	0.260	0.0372	0.0084	1	0.0137	0.00056	$1.57\ 10^{-5}$
5.06	0.258	0.0334	0.0077	1	0.0178	0.00062	$1.77\ 10^{-5}$
10.11	0.255	0.0344	0.0081	1	0.0199	0.00077	$1.90\ 10^{-5}$
15.15	0.258	0.0347	0.0080	1	0.0209	0.00086	$1.82\ 10^{-5}$
35.29	0.246	0.0297	0.0064	1	0.0159	0.00069	$1.68\ 10^{-5}$
55.34	0.242	0.0257	0.0057	1	0.0127	0.00061	$1.90\ 10^{-5}$
105.1	0.249	0.0293	0.0061	1	0.0188	0.00101	$2.10\ 10^{-5}$
203.2	0.249	0.0253	0.0046	1	0.0222	0.00159	$3.05\ 10^{-5}$
440.3	0.241	0.0223	0.0042	1	0.0207	0.00151	$2.92\ 10^{-5}$
1088	0.240	0.0201	0.0037	1	0.0301	0.00326	$6.34\ 10^{-5}$
1285	0.250	0.0208	0.0037	1	0.0294	0.00311	$6.46\ 10^{-5}$

photoluminescence of the initial sample is due to direct radiative exciton recombination, a fraction that levels of at 64% at the highest concentrations of $BuNH_2$ added.

Table S4: Relative contribution of each decay component to the photoluminescence.

[$BuNH_2$]	f_1	f_2	f_3
0	0.95	0.04	0.01
2.53	0.90	0.09	0.02
5.06	0.86	0.12	0.02
10.11	0.85	0.13	0.02
15.15	0.85	0.13	0.02
35.29	0.86	0.11	0.02
55.34	0.87	0.10	0.02
105.1	0.83	0.13	0.03
203.2	0.77	0.17	0.07
440.3	0.76	0.17	0.07
1088	0.64	0.23	0.13
1285	0.64	0.23	0.13

References

(1) Tomar, R.; Kulkarni, A.; Chen, K.; Singh, S.; van Thourhout, D.; Hodgkiss, J. M.; Siebbeles, L. D. A.; Hens, Z.; Geiregat, P. *J. Phys. Chem. C* **2019**, *123*, 9640–9650.

(2) Achtstein, A. W.; Antanovich, A.; Prudnikau, A.; Scott, R.; Woggon, U.; Artemyev, M. *J. Phys. Chem. C* **2015**, *119*, 20156–20161.

(3) Akoka, S.; Barantin, L.; Trierweiler, M. *Anal. Chem.* **1999**, *71*, 2554–2557.

(4) Perdew, J. P.; Burke, K.; Ernzerhof, M. *Phys. Rev. Lett.* **1997**, *78*, 1396–1396.

(5) VandeVondele, J.; Hutter, J. *J. Chem. Phys.* **2007**, *127*, 114105.

(6) Hutter, J.; Iannuzzi, M.; Schiffmann, F.; VandeVondele, J. *Wiley Interdiscip. Rev. Comput. Mol. Sci.* **2014**, *4*, 15–25.